Journal of Applied Fluid Mechanics, Vol. 9, No. 2, pp. 565-572, 2016.
Available online at www.jafmonline.net, ISSN 1735-3572, EISSN 1735-3645.
DOI: 10.18869/acadpub.jafm.68.225.24665

Influence of Magnetic Field and Slip on Jeffrey Fluid in a Ciliated Symmetric Channel with Metachronal Wave Pattern

N. S. Akbar[1], Z. H. Khan[2] and S. Nadeem[3†]

[1]*DBS&H CEME, National University of Sciences and Technology, Islamabad Pakistan*
[2]*Department of Mathematics, University of Malakand, Khyber, Pakhtunktwa 18800, Pakistan*
[3]*Department of Mathematics, Quaid-i-Azam University 45320, Islamabad 44000 Pakistan*

†*Corresponding Author Email: snqau@hotmail.com*

(Received February 1, 2015; accepted March 28, 2015)

ABSTRACT

The instinct system of cilia motion with magnetic field and slip for Jeffrey fluid model in a symmetric channel is examined. The problem of two-dimensional fluid motion in a symmetric channel with ciliated walls is considered. The structures of ciliary motion are stubborn by the sovereignty of viscid possessions above inertial properties by the long-wavelength and low Reynolds approximation. Exact solutions for the longitudinal pressure gradient, temperature and velocities are obtained. The pressure gradient and volume flow rate for different values of the flow parameters are also discussed. The flow property for the Jeffrey fluid is presented graphically as a function of the cilia and metachronal wave velocity.

Keywords: Magnetic field; Ciliary motion; Symmetric channel; Jeffrey fluid; Thermal and velocity slip; Exact solutions.

NOMENCLATURE

a	wave's amplitudes	γ	thermal slip parameter.
B_r	brinkman number	ε	cilia length
c	wave speed	ν	kinematic viscosity of the fluid
F	flow rate	μ	viscosity of the fluid
M	Hartmann number	Λ	velocity slip parameter
p_y	yield stress	Θ, T	temperature
Re	modified Reynolds number	λ_1	ratio of relaxation to retardation time
t	time	α	eccentricity of the elliptical motion
U,V	velocity components	β	slenderness parameter
X,Y	coordinates		

1. INTRODUCTION

Membrane-enclosed motile structure extending from the surface of eukaryotic cells. Cilia usually occur in groups and beat rhythmically to move a cell (e.g., single-celled organism) or to move small particles or fluid along the surface (e.g., trachea cells). Ciliary and flagellar beating is characterized by a series of bends, originating at the base of the structure and propagated toward the tip. High-speed strobe microscopy allows the waveform of the beat. Virtually all eukaryotic cilia and flagella are remarkably similar in their organization, possessing a central bundle of microtubules, called the axoneme, in which nine outer doublet microtubules surround a central pair of singlet microtubules (Gray and Hancock,1955; Dillon et al., 2007). Very recently Akbar and Butt (2015) analyzed the effect of heat transfer in a flexible tube with ciliated walls and carbon nanotubes. The problem has been formulated in the form of non-linear partial differential equations, after simplification exact solutions are evaluated for velocity and temperature profile. They observed that the change in throughout pure water is more

than that of Cu-water as the Hartmann number increases for both the single- and multi-walled carbon nanotubes case. In other articles Akbar *et al*. (2014), presented metachronal beating of cilia under influence of hartmann layer and heat transfer with copper nano fluids. They observed that the magnitude of the pressure gradient increases with the increase in the slenderness parameter, the Hartman number, the eccentricity of the elliptic motion and the cilia length. They also analyzed that the temperature is greater for pure water as compare to Cu-water and with high nanoparticle fraction it starts decreasing. Heat transfer analysis of bi-viscous ciliary motion fluid is quoted by Akbar and Khan (2014). According to them the velocity field increases uniformly with the increase in slenderness parameter.

Although in the cilia problems less attention have been given to analyze the flows in the presence of a slip conditions. The application of slip condition in such flows has special relevance in physiology and polymers. It is now known that the no-slip conditions for velocity and the thermal conditions are not appropriate for momentum and heat transfer in micro devices. The velocity slip and temperature jump conditions are adequate for the flow of liquids at the micro scale level especially in view of the lack of data on the thermal accommodation coefficient. Among the application of micro devices, several complex micro channels arise. For instance, the micro conducts of rectangular, triangular or trapezoidal cross section are very popular and easier to manufacture in the micro scale thermal fluid system see Reference.

The problem of two-dimensional motion of Jeffrey fluid and heat transfer in a planner channel with ciliated walls is considered. The features of ciliary structures are resolute by the supremacy of viscous effects above inertial possessions by the long-wavelength and low Reynolds approximation. This is the first article in literature to discuss heat transfer for ciliary motion. Closed-form solutions for the longitudinal pressure gradient, temperature and velocities are obtained. The pressure gradient and volume flow rate for different values of the flow parameters are also premeditated. Streamlines and Isotherms are displayed for the understating of the proposed model.

2. FLOW EQUATION

We consider an incompressible MHD Jeffrey fluid in a planner channel. Channel is ciliated with metachronal wave pattern which propagates along the wall of the channel. The *y*-coordinate is measured along the channel, where *x*-coordinate transverse to it. The magnetic field B_0 is imposed on the flow in the *x*-direction normal to the flow. It is assumed that the wall of the channel is heated uniformly at a constant temperature T_0 with symmetry at center. The physical model and coordinate system are shown in Fig. 1.

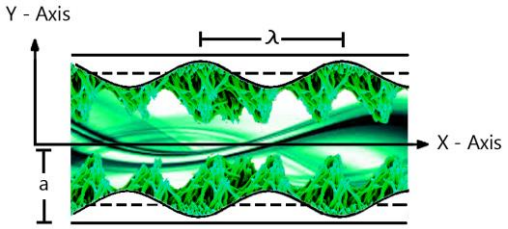

Fig.1. A physical sketch of ciliated channel.

The geometry of the metachronal wave form proposes that the covering of the cilia advices can be stated precisely as

$$Y = f(X,t) = \pm\left[a + a\varepsilon\cos\left(\frac{2\pi}{\lambda}(X - ct)\right)\right] = \pm L = \pm H \tag{1}$$

Sleigh [2,3] observed that cilia tips move in elliptical paths; therefore, the horizontal position of the cilia tips can be written as

$$X = g(X,t) = X_0 + \varepsilon\alpha a\sin\left(\frac{2\pi}{\lambda}(X - ct)\right) \tag{2}$$

The horizontal and vertical velocities of the cilia are given as [2, 3]

$$U_0 = \frac{-\left(\frac{2\pi}{\lambda}\right)\varepsilon\alpha ac\cos\left(\frac{2\pi}{\lambda}(X - ct)\right)}{1-\left(\frac{2\pi}{\lambda}\right)\varepsilon\alpha ac\cos\left(\frac{2\pi}{\lambda}(X - ct)\right)} \tag{3}$$

$$V_0 = \frac{-\left(\frac{2\pi}{\lambda}\right)\varepsilon\alpha ac\sin\left(\frac{2\pi}{\lambda}(X - ct)\right)}{1-\left(\frac{2\pi}{\lambda}\right)\varepsilon\alpha ac\sin\left(\frac{2\pi}{\lambda}(X - ct)\right)} \tag{4}$$

The expression for fixed and wave frames are related by the following relations

$$\bar{x} = \bar{X} - ct,\ \bar{y} = \bar{Y},\ \bar{u} = \bar{U} - c,\ \bar{v} = \bar{V},\ p(\bar{x}) = P(\bar{X},t)$$
. (5)

Introducing the following non-dimensional quantities

$$x = \frac{2\pi\bar{x}}{\lambda},\ y = \frac{\bar{y}}{a},\ u = \frac{\bar{u}}{c},\ v = \frac{\bar{v}}{c},\ t = \frac{2\pi\bar{t}}{\lambda},\ \beta = \frac{2\pi d_1}{\lambda},$$
$$P = \frac{2\pi a^2\bar{P}}{\mu c\lambda},\ h = \frac{\bar{h}}{a},\ \mathrm{Re} = \frac{\rho ca}{\mu},\ S = \frac{\bar{S}a}{\mu c},\ \theta = \frac{\bar{T} - \bar{T}_0}{\bar{T}_0},$$
$$B_r = P_r E_c,\ E_c = \frac{c^2}{c_p\bar{T}_0},\ P_r = \frac{\mu c_p}{k}. \tag{6}$$

The stream function and velocity field are related by the expressions

$$u = \frac{\partial\Psi}{\partial y},\ v = -\delta\frac{\partial\Psi}{\partial x}. \tag{7}$$

Under the long wavelength and low Reynolds number assumption, the dimensionless governing equations take the following form

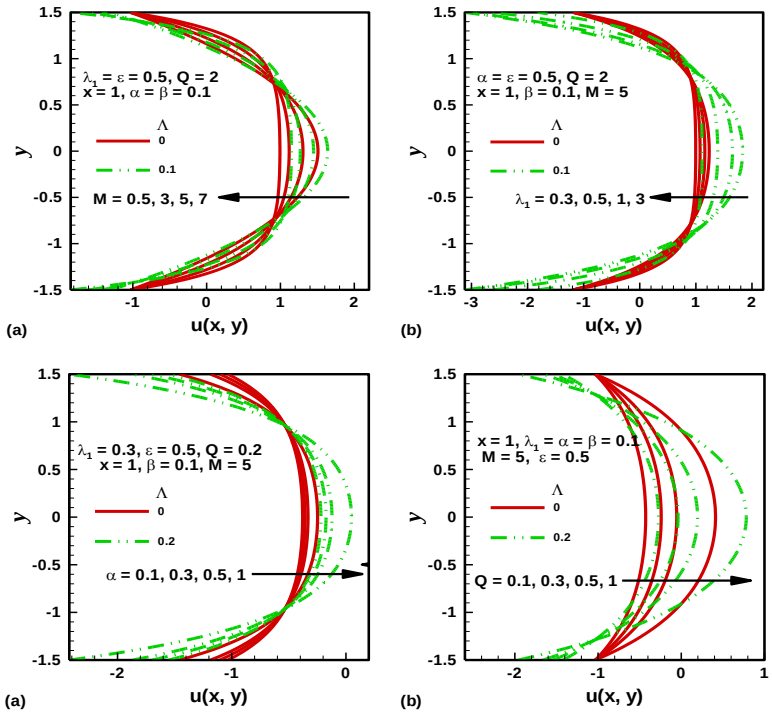

Fig. 2. Velocity profile along *y*-axes for different flow parameters.

$$\left(\frac{1}{1+\lambda_1}\right)\frac{\partial^2 u}{\partial y^2} - M^2(u+1) = \frac{dP}{dx}, \tag{8}$$

$$\frac{\partial^2 \theta}{\partial y^2} = -B_r\left(\frac{1}{1+\lambda_1}\right)\left(\frac{\partial u}{\partial y}\right)^2 \tag{9}$$

Corresponding boundary conditions are

$$\frac{\partial u}{\partial y} = 0, \quad \frac{\partial \theta}{\partial y} = 0 \quad \text{at} \quad y = 0,$$

$$u = -1 - \frac{2\pi\varepsilon\alpha\beta_1\cos(2\pi x)}{1-2\pi\varepsilon\alpha\beta_1\cos(2\pi x)} + \left(\frac{\Lambda}{1+\lambda_1}\right)\frac{\partial u}{\partial y}, \tag{10}$$

$$\theta + \gamma\frac{\partial \theta}{\partial y} = 0 \text{ at } y = h = 1 + \varepsilon\cos(2\pi x), \tag{11}$$

The flow rates in fixed and wave frame are related by [14]

$$Q = F + 1 \tag{12}$$

3. SOLUTION OF THE PROBLEM

The moment equation (8) for the proposed model is a second order linear differential equation, which has a closed-form solution

$$u(x,y) = C_1 e^{-M\sqrt{1+\lambda_1}y} + C_2 e^{M\sqrt{1+\lambda_1}y} - 1 - \frac{1}{M^2}\frac{dp}{dx} \tag{13}$$

The constants of integration C_i, $i = 1,\ 2$ are obtained using boundary conditions (10) and (11) through Mathematica 9. A closed form expression for the pressure gradient is,

$$\frac{dP}{dx} = \left(-e^{-Mh\sqrt{1+\lambda_1}} + 1\right)\frac{MC_1}{h\sqrt{1+\lambda_1}} + \left(e^{Mh\sqrt{1+\lambda_1}} - 1\right)\frac{MC_2}{h\sqrt{1+\lambda_1}} - \left(1+\frac{F}{h}\right)M^2 \tag{14}$$

The dimensionless pressure rise is obtained by substituting (11) into the following equation

$$\Delta P = \int_0^1 \left(\frac{dP}{dx}\right)dx\,. \tag{15}$$

The energy equation (9) has also a closed-form solution

$$\theta(x,y) = \Omega_1 + \Omega_2 y - \left(1+\lambda_1\right)B_r M^4 \left[\frac{1}{4}\frac{1}{M^2\left(1+\lambda_1\right)}\left\{C_1^2 e^{-2M\sqrt{1+\lambda_1}y} + C_2^2 e^{2M\sqrt{1+\lambda_1}y}\right\} + C_1 C_2 y^2\right] \tag{16}$$

where Ω_1 and Ω_2 are constants of integration, which are obtained using boundary conditions (10) and (11).

4. RESULTS AND DISCUSSION

In this section, the effects of the different flow parameters, such as the slenderness parameter β, Hartman number M , eccentricity of the elliptic

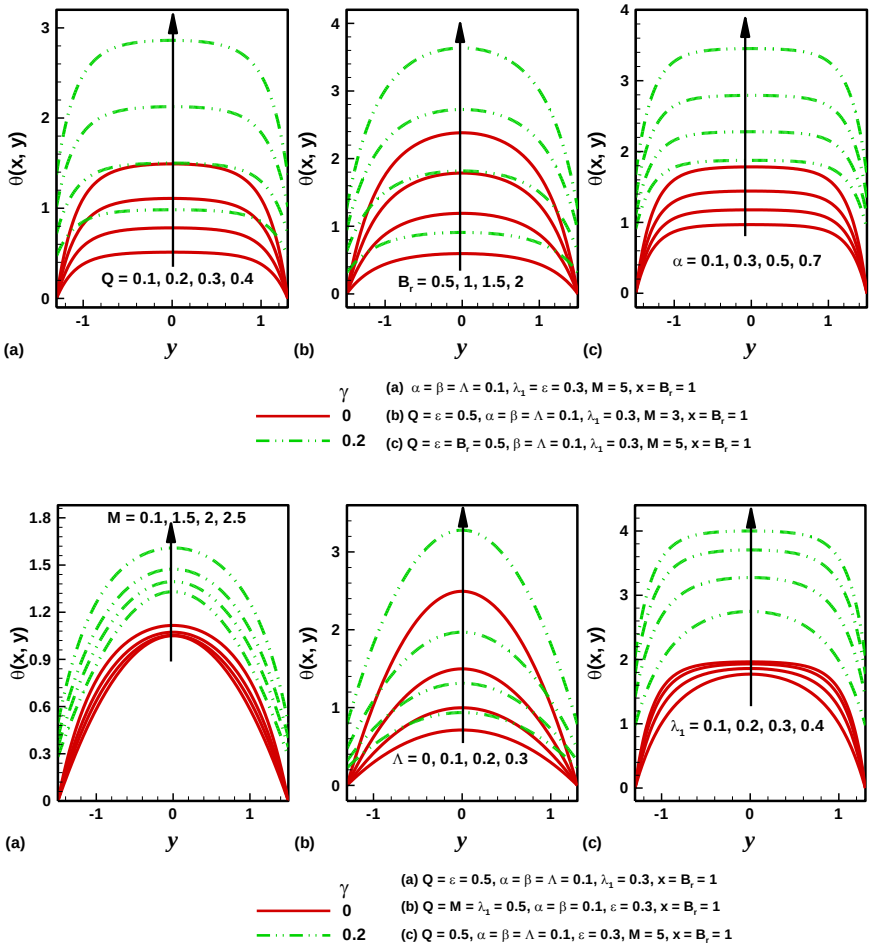

Fig. 3 Temperature profile along *y*-axes for different flow parameters.

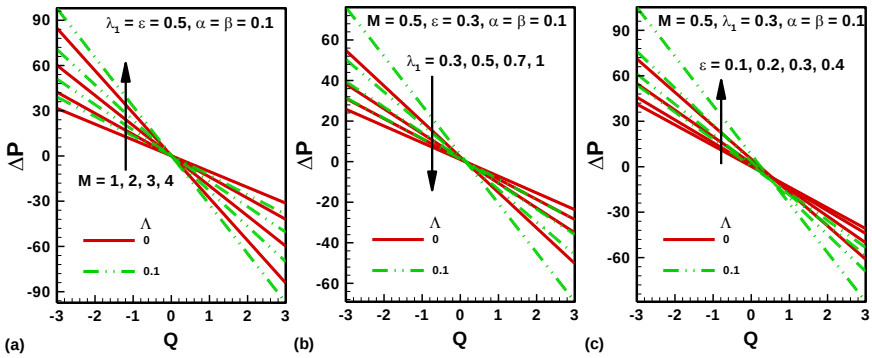

Fig. 4. Variations in pressure rise versus flow rate for different flow governing parameters.

motion α, flow rate Q, ratio of relaxation to retardation time λ_1 and cilia length ε on the pressure rise, pressure gradient, velocity, temperature, streamlines and isotherms has been discussed and physically interpreted.

4.1 Flow Characteristics

The velocity field is illustrated in the Fig. 2(a-d), for different values of ratio of relaxation to retardation time λ_1 with change in Hartmann number *M*, eccentricity of the elliptic motion α and flow rate *Q* for both slip and no slip case. It is seen that velocity field decreases at the center of the channel by increase in ratio of relaxation to retardation time λ_1 and Hartmann number *M* but near the channel walls behavior is different i.e. velocity field decreases for increase in ratio of relaxation to retardation time λ_1 and Hartmann number *M*. Influence of eccentricity of the elliptic motion α and flow rate *Q* on velocity profile is different as compare to ratio of relaxation to retardation time λ_1 and Hartmann number *M*. Velocity profile increases at the center of the channel but decreases near the channel walls by rise in eccentricity of the

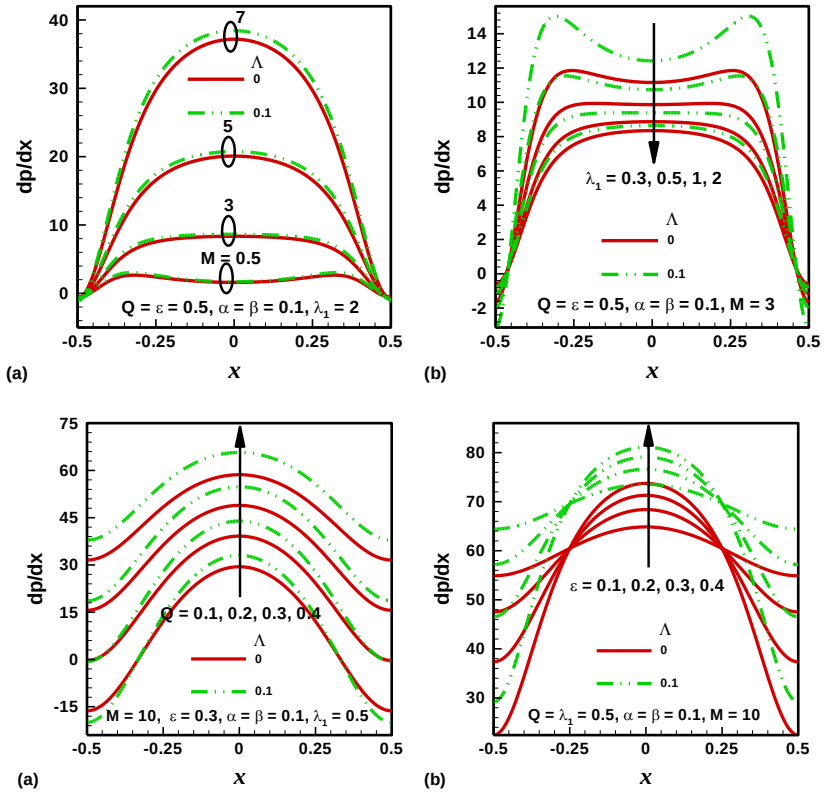

Fig. 5. Influence of the governing parameters on the pressure gradient along *x*-axes.

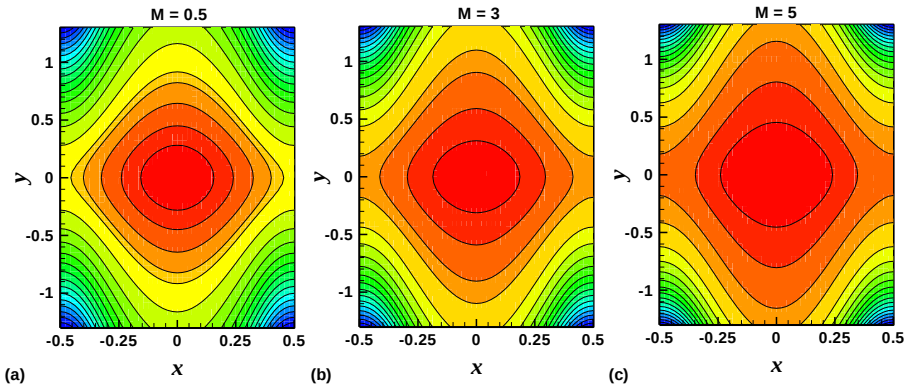

Fig. 6. Variations in streamlines with the Hartmann number M.

elliptic motion α and flow rate *Q*. It is also seen that velocity for the case of slip is high for all the parameters as compare to the no slip case. Temperature profile is displayed in Figs. 3(a-e). It is observed that for different values of ratio of relaxation to retardation time λ_1 , Hartmann number M , flow rate Q, Brinkman number B_r, velocity slip parameter Λ and eccentricity of the elliptic motion α temperature field increases in whole channel . It is also analyzed the temperature rise rapidly for thermal slip case as compare to no thermal slip.

4.2 Pumping Characteristics

Numerical integration is performed for the pressure rise per wave-length. It is noticed that the pressure rise and volume flow rate have opposite behaviours. From Figs. 4(a-c). It is found that in pumping region $(\Delta P > 0)$, the pressure rise decreases with the increase of ratio of relaxation to retardation time λ_1, while pressure rise increase with the increase in Hartmann number *M* and cilia length $\mathcal{E}$. Figs. 4(a) to 4(c) also show that in the augmented pumping region for $\Delta P < 0$, pressure rise gives the opposite results for all the parameter as compared to the pumping region $(\Delta P > 0)$. Free pumping region holds for $\Delta P = 0$. Moreover Pressure rise increases rapidly for velocity slip case as compare to no slip case.

The pressure gradient for different values of the flow parameters is plotted in the Fig. 5(a-d). Magnitude of pressure gradient decreases with the increase in the ratio of relaxation to retardation time

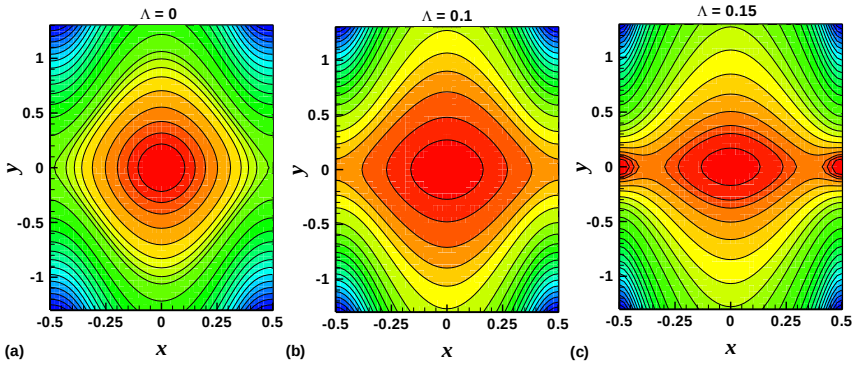

Fig. 7. Effects of the slip parameter on the streamlines.

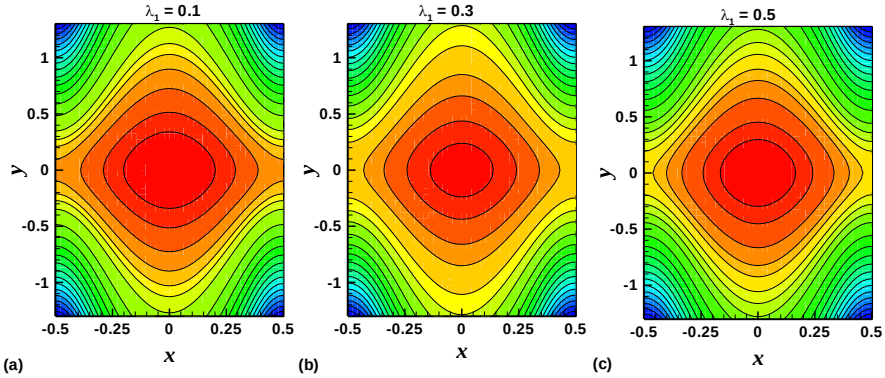

Fig. 8. Effects of the ratio of relaxation to retardation time λ_1 on the Isotherms.

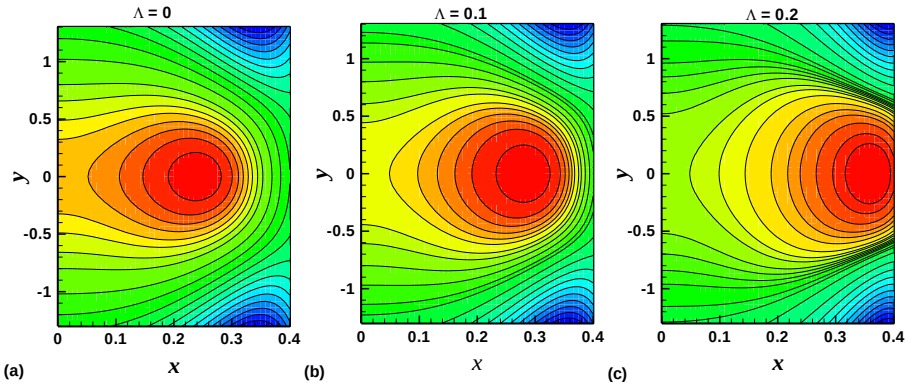

Fig. 9. Effects of the velocity slip parameter on the Isotherms.

λ_1 but increases for increasing values of Hartmann number M flow rate Q and cilia length $\mathcal{E}$. It is also observed that the maximum pressure gradient occurs when x=0.48 and near the channel walls the pressure gradient is small. This leads to the fact that flow can easily pass in the middle of the channel. Again it is seen that pressure gradient is high for velocity slip case as compare to no slip

4.3 Trapping Phenomena and Isotherms

The trapping phenomena for different values of Hartmann number M is shown through Fig. (6a) to (6c). It is seen that for large values of Hartmann number M, size of the bolus increases but number of bolus decreases, From Figs. 7 display that for increasing slip parameter size and number of bolus both decreases. Streamlines for ratio of relaxation to retardation time λ_1 are shown in the Figs. (8a) to (8c). Fig 8, shows that with an increase in λ_1 size of the trapping bolus decreases but number of bolus increases.

A line connecting points of equal temperature is called an isotherm. From Figs. 8 and 9, the small orange numbers are contour labels, which identify the value of an isotherm (75, 85 degrees Fahrenheit). So it analyzed that when we increases velocity slip parameter then temperature is going less than 75, 85 Fahrenheit, but with the increase in thermal slip parameter than temperature is 75, 85 degrees Fahrenheit See Figs. 9 and 10.

5 CONCLUSIONS

Impact of thermal and velocity slip for Jeffrey fluid

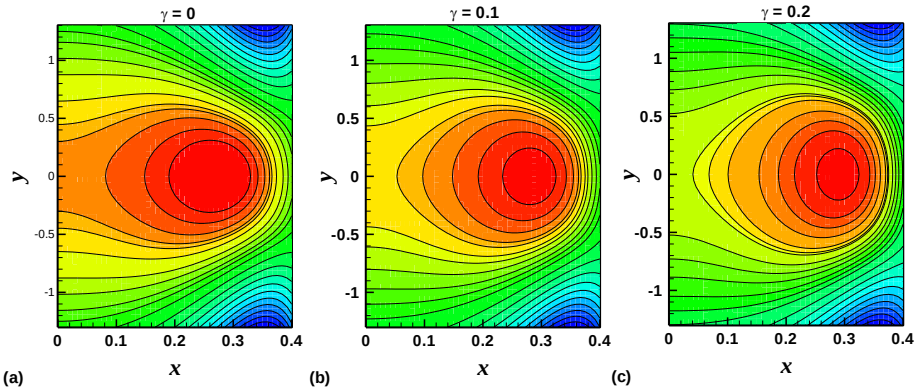

Fig. 10. Effects of the thermal slip parameter on the Isotherms.

in a ciliated symmetric channel with metachronal wave pattern is discussed. Key points of the performed analysis are as follows:

- It is seen that velocity field decreases at the center of the channel by increase in ratio of relaxation to retardation time λ_1 and Hartmann number *M*.
- Velocity profile increases at the center of the channel but decreases near the channel walls by rise in eccentricity of the elliptic motion α and flow rate *Q*.
- It is observed that for different values of ratio of relaxation to retardation time λ_1 , Hartmann number M , flow rate Q, Brinkman number B_r, velocity slip parameter Λ and eccentricity of the elliptic motion α temperature field increases in whole channel.
- It is also analyzed the temperature rise rapidly for thermal slip case as compare to no thermal slip.
- The pressure rise decreases with the increase of ratio of relaxation to retardation time λ_1, while pressure rise increase with the increase in Hartmann number *M* and cilia length $\mathcal{E}$.
- Free pumping region holds for $\Delta P = 0$.
- Pressure rise increases rapidly for velocity slip case as compare to no slip case.
- Magnitude of pressure gradient decreases with the increase in the ratio of relaxation to retardation time λ_1 but increases for increasing values of Hartmann number *M*, flow rate Q and cilia length ε .
- With an increase in λ_1 size of the trapping bolus decreases but number of bolus increases.
- It analyzed that when we increases velocity slip parameter then temperature is going less than 75, 85 Fahrenheit, but with the increase in thermal slip parameter than temperature is 75, 85 degrees Fahrenheit

REFERENCES

Akbar, N. S. and A. W. Butt (2014). CNT suspended nanofluid analysis in a flexible tube with ciliated walls. *Eur. Phys. J. Plus* 129,174.

Akbar, N. S., Z. H. Khan and S. Nadeem (2014). Metachronal beating of cilia under influence of Hartmann layer and heat transfer. *Eur. Phys. J. Plus* 129,176.

Akbar, N. S., A. W. Butt and N. F. M. Noor (2014). Heat transfer analysis on transport of copper nanofluids due to metachronal waves of cilia. *Current Nano Sciences* 10, 807-815.

Akbar, N. S. and Z. H. Khan (2015). Heat transfer analysis of bi-viscous ciliary motion fluid. *Int. J. Biomathematics*, 8, 1550026 (13 pages).

Akbar, N. S. and A. W. Butt (2015). Heat Transfer Analysis for the Peristaltic Flow of Herschel--Bulkley Fluid in a Nonuniform Inclined Channel. *Zeitschrift für Naturforschung A.* 70, 23-32.

Akbar, N. S., Z. H. Khan and S. Nadeem (2014). Metachronal beating of cilia under influence of Hartmann layer and heat transfer. *Eur. Phys. J. Plus* 129, 176.

Akbar, N. S. and S. Nadeem (2014). Convective heat transfer of a Sutterby fluid in an inclined asymmetric channel with partial slip. *Heat transfer research*, 45(3) ,219-240.

Akbar, N. S. and Z. H. Khan (2014). Heat transfer analysis of the peristaltic instinct of biviscosity fluid with the impact of thermal and velocity slips. *International Communications in Heat* and Mass Transfer 58, 193-199.

Akbar, N. S. (2014) . Biological analysis of nano Prandtl fluid model in a diverging tube. *Journal of computational and theoretical nanosciences* 12, 105-112.

Akbar, N. S. (2014) . Peristaltic flow of Cu-water nanofluid in a tube. *Journal of computational and theoretical nanosciences* 11, 1411−1416.

Akbar, N. S. (2015). Application of Eyring-Powell fluid model in peristalsis with nano particles. *Journal of computational and theoretical nanosciences* 12, 94-100.

Dillon, R. H., L. J. Fauci, C. Omoto and X. Yang

(2007). Fluid Dynamic Models of Flagellar and Ciliary Beating, Ann. N. Y. *Acad. Sci.* 1101, 494-505.

Ghasemi, J. and S. E. Razavi (2013). Numerical Nanofluid Simulation with Finite Volume Lattice-Boltzmann Enhanced Approach. *Journal of Applied Fluid Mechanics* 6, 519-527.

Gray, J. and G. Hancock (1955). The propulsion of sea-urchin spermatozoa. *J. Exp. Biol.* 32, 802-814.

Gueron, S. and N. Liron (1992). Ciliary motion modeling, and dynamic multicilia interactions. *Biophys J. Oct 63*(4), 1045-1058.

Gueron, S. and K. Levit-Gurevich (1998). Computation of the Internal Forces in Cilia: Application to Ciliary Motion, the Effects of Viscosity, and Cilia Interactions. *Biophysical Journal*, 74, 1658-1676.

Ramiar, A. , A. A. Ranjbar and S. F. Hosseinizadeh (2012) . Effect of Axial Conduction and Variable Properties on TwoDimensional Conjugate Heat Transfer of Al2O3-EG/Water Mixture Nanofluid in Microchannel. *Journal of Applied Fluid Mechanics* 5,79 – 87.

Rashad, A. M., A. J. Chamkha and M. M. M. Abdou (2013). Mixed Convection Flow of Non-Newtonian Fluid from Vertical Surface Saturated in a Porous Medium Filled with a Nanofluid. *Journal of Applied Fluid Mechanics* 6, 301-309.

Sleigh, M. A. (1962). *The Biology of Cilia and Flagella*, MacMillian, New York.

Sleigh, M. A. (1968), *Patterns if Ciliary Beating*, *In Aspects of Cell Motility*, Soc Expl Biol Sump XX I I, Academic Press, New York.